Salvador, FJ.; Jaramillo-Císcar, D.; Romero, J.; Roselló, M. (2017). Using a homogeneous equilibrium model for the study of the inner nozzle flow and cavitation pattern in convergent-divergent nozzles of diesel injectors. Journal of Computational and Applied Mathematics. 309:630-641. doi:10.1016/j.cam.2016.04.010

USING A HOMOGENEOUS EQUILIBRIUM MODEL FOR THE STUDY OF THE INNER NOZZLE FLOW AND CAVITATION PATTERN IN CONVERGENT-DIVERGENT NOZZLES OF DIESEL INJECTORS.

F.J. Salvador[1], D. Jaramillo[1], J.-V. Romero[2] and M.-D. Roselló[2]

[1]CMT-Motores Térmicos,
Universitat Politècnica de València,
Camino de Vera, s/n, Edificio 6D
46022 Valencia, España

[2]Instituto de Matemática Multidisciplinar,
Universitat Politècnica de València,
Camino de Vera, s/n, Edificio 8G, 2º
46022 Valencia, España

(*) Corresponding author:

Dr. F. Javier Salvador, fsalvado@mot.upv.es

CMT-Motores Térmicos, Universitat Politècnica de València

Camino de Vera s/n, E-46022, Valencia, Spain

Telephone: 34-963879659

Fax: 34- 963877659

ABSTRACT

In this paper, the behaviour of the internal nozzle flow and cavitation phenomenon are numerically studied for non-conventional Diesel convergent-divergent nozzles in order to assess their potential in terms of flow characteristics. The used nozzles differs each other in the convergence-divergence level of the orifices but all of them keep the same diameter at the middle of the nozzle orifice. The calculations have been performed using a code previously validated and able to simulate cavitation phenomenon using a homogeneous equilibrium model for the biphasic fluid and using a RANS method (RNG k-ε) as a turbulence modelling approach. For the simulations, one injection pressure and different discharge pressures were used in order to assess the characteristics of nozzles for different Reynolds conditions involving cavitating and non-cavitating conditions.

The comparison of the nozzles has been carried out in terms of flow characteristics such as mass flow, momentum flux, effective velocity and other important dimensionless

parameters which help to describe the behaviour of the inner flow: discharge coefficient (C_d), area coefficient (C_a) and velocity coefficient (C_v). Additionally, the nozzles have been compared in terms of cavitation inception conditions and cavitation development.

The study has shown a high influence on the results of the level of convergence-divergence used in the nozzles. In these nozzles, the vapour originated from cavitation phenomenon came from the throttle of the orifice at the midpoint, and it extended along the whole wall of the divergent nozzle part towards the outlet of the orifice. The main results of the investigation have shown how the different geometries modify the cavitation conditions as well as the discharge coefficient and effective velocity. In particular, the nozzle with highest convergence-divergence level showed cavitation for all the tested conditions while for the nozzle with lowest convergence-divergence level, the cavitation phenomenon could be avoided for high discharge pressures. Additionally, the nozzle with highest convergence-divergence level showed the lowest discharge coefficient values but similar effective injection velocity than the nozzle with lowest level of convergence-divergence level despite of its higher orifice outlet area.

Keywords: cavitation; OpenFOAM®; internal flow; diesel injector; nozzle; CFD; convergent-divergent nozzle;

1. INTRODUCTION

One of the most important processes controlling the combustion efficiency and pollutants formation in Diesel engines is the air-fuel mixing process. The air-fuel mixing process depends on the spray characteristics, which in turn depends on the geometry of the nozzle and the injection pressure conditions, among other factors [1–5]. With the aim of studying

new ways for improving the fuel-air mixing process and, therefore, the combustion process, non-conventional nozzle orifices have been studied in the last years [6–11]. These studies were conducted in order to study the potential of elliptical nozzles, and in general terms, it was demonstrated that air entrainment of jets injected into gas is considerably increased if elliptic orifices are used instead of circular orifices [6, 7]. This was mainly due to the higher injection velocity related to higher cavitation intensity in this type of nozzles in addition to the wider spray cone angle [8]. Nevertheless, the investigations in the literature aiming at quantifying the potential of convergent-divergent orifices in diesel nozzles are scarce. These geometries have been used for other applications different from diesel nozzles such as acoustic [12] and refrigeration systems [13].

The aim of this study is to increase the available information on this type of non-conventional orifices in diesel injector nozzles in order to assess their potential to enhance the air-mixing process by means of Computational Fluid Dynamics (CFD). The assessment has been performed by evaluating the inner flow characteristics for three different nozzles with different convergence-divergence level. Mass flow, momentum flux, effective velocity and other important non-dimensional parameters, which help to describe the behaviour of the inner flow, have been used for the nozzles assessment. Additionally, the nozzles have been also compared in terms of cavitation inception conditions and development, which in turn is strongly related to the flow characteristics.

The calculations have been performed using a code previously validated and able to simulate cavitation phenomenon using a Homogeneous Equilibrium Model (HEM) for the biphasic fluid and a RANS (Reynolds Averaged Navier-Stokes) method (RNG k-ε)

as a turbulence modelling approach. For the simulations, as a first step, one injection pressure and different discharge pressures simulating the pressure in the combustion chamber were used in order to compare the nozzles for different Reynolds conditions and in cavitating and non-cavitating conditions.

The present paper has been divided into 5 sections. First of all, a complete description of the computational fluid dynamics approach used to study the inner nozzle flow and cavitation phenomenon is performed in Section 2. The geometry characteristics of the three convergent-divergent nozzles and the boundary conditions used for the simulations are explained in Section 3. The main results are presented and analysed in Section 4, and finally, the main conclusions are drawn in Section 5.

2. DESCRIPTION OF THE CFD APPROACH

2.1 Cavitation modelling

The code used in the present study for modelling cavitating flows is implemented in OpenFOAM ® [14]. This model, validated in calibrated orifices, one-hole and multi-hole nozzles by Salvador et al. in its laminar [2, 5, 15, 16], turbulent RANS [4] and LES [17] versions belongs to the homogeneous equilibrium models (HEM).

In HEM models, the assumptions of local kinematic equilibrium (local velocity is the same for both phases) and local thermodynamic equilibrium (temperature, pressure and free Gibbs enthalpy equality between phases) are made. This kind of model cannot reproduce strong thermodynamic or kinetic non-equilibrium effects, but it is often used for numerical simulations due to its simplicity and numerical stability. These two advantages are the main reasons why this model was chosen by the authors.

The homogeneous equilibrium model calculates the growth of cavitation using a barotropic equation of state (Eq. (1)), which relates pressure and density through the compressibility of the mixture, being the compressibility the inverse of the speed of sound squared (Eq. (2)):

$$\left(\frac{\partial\rho\left(t,P(\vec{x},t)\right)}{\partial P}\right)_t = \Psi \tag{1}$$

$$\Psi = \frac{1}{c^2} \tag{2}$$

The amount of vapour in the fluid is calculated with the void fraction γ (Eq. (3)), which is 0 in a flow without cavitation and 1 for fully cavitating flows.

$$\gamma = \max\left(\min\left(\frac{\rho - \rho_{\mathrm{l,sat}}}{\rho_{\mathrm{v,sat}} - \rho_{\mathrm{l,sat}}}, 1\right), 0\right) \tag{3}$$

The compressibility of the mixture (Eq. (4)) is calculated from Ψ_{v} and Ψ_{l} (vapour and liquid compressibility, respectively) using a linear model.

Despite the fact that there are models which describe the compressibility of the mixture in a more physical way like the models of Chung [18] or Stewart [19], a linear model was chosen based on the better convergence of the results and their stability [2]:

$$\Psi = \gamma\Psi_{\mathrm{v}} + (1-\gamma)\Psi_{\mathrm{l}} \tag{4}$$

In the case where there is only vapour or liquid, the following linear equation of state can be derived from Eq. (1) if the speed of sound is considered constant:

$$\rho_v = \Psi_v P \tag{5}$$

$$\rho_l = \rho_l^0 + \Psi_l P \tag{6}$$

The linear model has also been used to calculate the density and the viscosity of the mixture:

$$\rho = (1-\gamma)\rho_l^0 + \Psi P \tag{7}$$

$$\mu = \gamma\mu_v + (1-\gamma)\mu_l \tag{8}$$

The iteration process to numerically solve the fluid behaviour starts with the continuity equation (Eq. (9)) to get a provisional density:

$$\frac{\partial \rho}{\partial t} + \nabla \cdot (\rho \vec{u}) = 0 \tag{9}$$

According to previous studies performed by the authors [2], the divergence term $\nabla(\rho\vec{u})$ is discretized in the space by using a Gauss upwind scheme to improve the stability, whereas an implicit discretisation in time is used for the density in the divergence term. With respect to the partial derivative over time, an Euler scheme is used for time discretisation. When the provisional density is computed, preliminary values for γ and Ψ are determined using Eqs. (3) and (4).

The next step is the calculation of a predictor for the velocity from the momentum conservation equation (Eq. (10)). The same procedure as before is followed: an Euler scheme for the partial derivatives over time and a Gauss upwind scheme for the divergence terms.

$$\frac{\partial(\rho\vec{u})}{\partial t} + \nabla \cdot (\rho\vec{u} \cdot \vec{u}) = -\nabla P + \nabla \cdot \left(\mu(\nabla\vec{u} + \nabla\vec{u}^{\mathrm{T}})\right) \quad (10)$$

Then the continuity equation (Eq. (9)) is modified with the equation of state and the following equation is solved by an iterative PISO algorithm:

$$\frac{\partial(\Psi P)}{\partial t} - \left(\rho_{\mathrm{l}}^{0} + (\Psi_{\mathrm{l}} - \Psi_{\mathrm{v}})P_{\mathrm{vap}}\right)\frac{\partial}{\partial t} - P_{\mathrm{vap}}\frac{\partial\Psi}{\partial t} + \nabla \cdot (\rho\vec{u}) = 0 \quad (11)$$

When the continuity convergence has been reached, the variables ρ, γ and Ψ are updated using Eqs. (7), (4) and (3), and the PISO algorithm is started again until convergence.

The convergence criteria used for all the simulations run in the present study is based on the local continuity and the residuals of all the flow variables. The local continuity is defined as the sum of all the cell flux imbalances and remains always below 1e-8 for all the conditions simulated, which is a clear sign of the good convergence and stability of the code. The second criterion used to check the convergence of every simulation is the evolution of the residuals for each flow variable. The residuals are evaluated by substituting the current solution into the equation and taking the magnitude of the difference between the left and right hand sides and are forced to remain constant below 1e-8.

2.2 Turbulence modelling

The turbulence is modelled using a RANS (Reynolds-averaged Navier-Stokes) method. In the RANS methods the solution is split into an averaged solution and a fluctuating solution. In particular the RNG k-ε model [20] used for the present work uses the Boussinesq assumption to model the turbulent viscosity:

$$-\overline{u'_i u'_j} = \mu_t \left(\frac{\partial \overline{u_i}}{\partial x_j} + \frac{\partial \overline{u_j}}{\partial x_i} - \frac{2}{3} \frac{\partial \overline{u_k}}{\partial x_k} \delta_{ij} \right) - \frac{2}{3} k \rho \delta_{ij} \quad (12)$$

The eddy or turbulent viscosity is defined as:

$$\mu_t = \rho C_\mu \frac{k^2}{\varepsilon} \quad (13)$$

Where k and ε are the turbulent kinetic energy and the turbulence energy dissipation, respectively. Two transport equations are associated with these variables:

$$\frac{\partial \rho k}{\partial t} + \nabla \cdot \left(\rho k \overrightarrow{\overline{u}} \right) = \nabla \cdot [(\mu + \mu_t \alpha_k) \nabla k] + p_k - \rho \varepsilon \quad (14)$$

$$\frac{\partial \rho \varepsilon}{\partial t} + \nabla \cdot \left(\rho \varepsilon \overrightarrow{\overline{u}} \right) = \nabla \cdot [(\mu + \mu_t \alpha_\varepsilon) \nabla \varepsilon] + C_{\varepsilon 1} \frac{\varepsilon}{k} p_k - C_{\varepsilon 2}^o \rho \frac{\varepsilon^2}{k} \quad (15)$$

with:

$$C_{\varepsilon 2}^o = C_{\varepsilon 2} + \frac{C_\mu \eta^3 \left(1 - \frac{\eta}{\eta_0}\right)}{1 + \beta \eta^3} \quad (16)$$

The new variables are the production of turbulent kinetic energy (p_k), expansion parameter (η) and the mean strain modulus (S), defined as:

$$p_k = \mu_t S^2 \quad (17)$$

$$\eta = \frac{Sk}{\varepsilon} \quad (18)$$

$$S = \sqrt{2 S_{ij} S_{ij}} \quad (19)$$

The coefficients used in the RNG k-ε model correspond to the values given by Yakhot et al. [20]:

$C_{\varepsilon 1} = 1.42$

$C_{\varepsilon 2} = 1.68$

$\alpha_k = 1.39$

$\alpha_\varepsilon = 1.39$

$C_\mu = 0.0845$

$\eta_0 = 4.38$

$\beta = 0.012$

3. GEOMETRY AND BOUNDARY CONDITIONS

A multi-hole nozzle with 7 orifices has been used as a basis. Due to the symmetry of the geometry the full nozzle is reduced to only one of the seven orifices (51.4º). The orifices of the three convergent-divergent nozzles used for the present investigation consist in, as shown in the Fig. 1, an initial convergent part until the midpoint of the orifice and a divergent part from the middle until the outlet. For simplicity, the convergent and the divergent parts are selected to be symmetrical, so the inlet and the outlet diameters are the same. The geometrical characteristics of the orifices can be found in Table 1. The three nozzles have the same diameter value at the midpoint of the orifice.

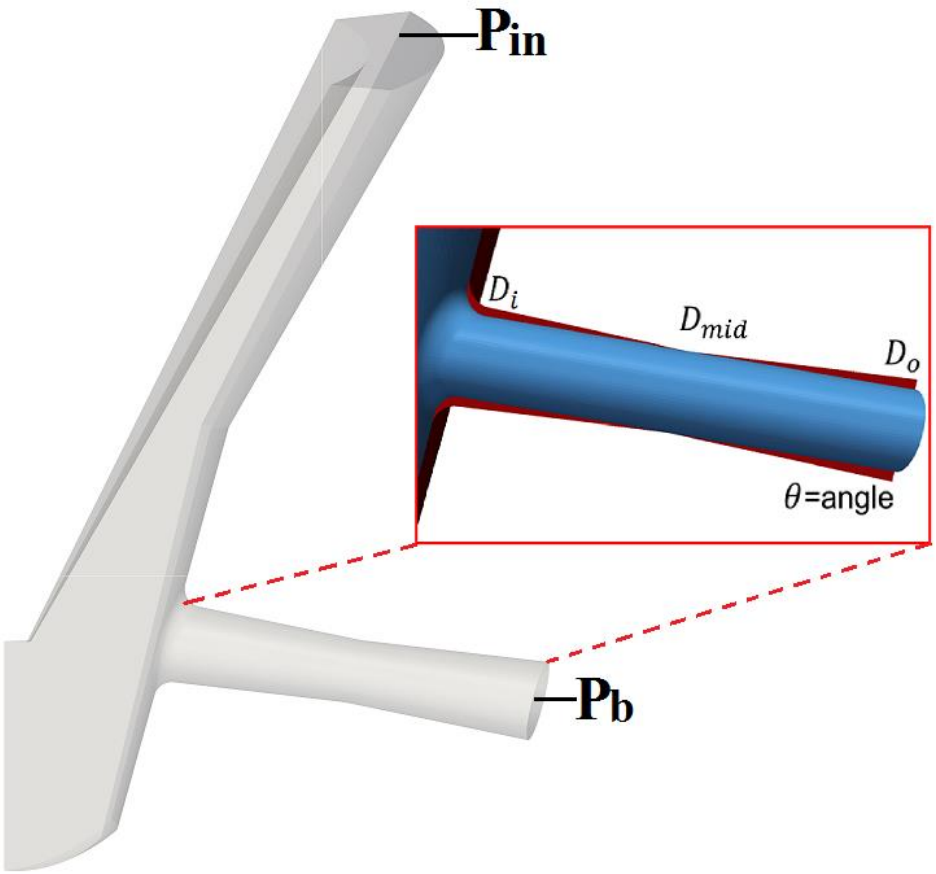

Figure 1: Nozzle´s geometry.

No	θ [º]	D_{mid} [µm]	D_{O} [µm]	$k-factor_{\text{con}}$ [−]
CD-2.5	2.5	124.6	156.3	3.2
CD-3.5	3.5	124.6	169.0	4.4
CD-4.5	4.5	124.6	181.7	5.7

Table 1: Geometrical characteristics of the nozzle´s orifices.

For the nozzle conicity factor, the standard definition of *k-factor* normally used in conical nozzles has been used [21]. So, for each part of the orifice, the conicity k-factor is defined as follows:

$$k - factor_{\text{con}} = \frac{D_i - D_{\text{mid}}}{10\ \mu\text{m}} \quad (20)$$

$$k - factor_{\text{div}} = \frac{D_{\text{mid}} - D_o}{10\ \mu\text{m}} \quad (21)$$

As the inlet and the outlet diameters are the same both k-factors have the same absolute value but different sign. For that reason, any reference to the k-factor will be in absolute value.

The meshing process of the geometries has been performed according to the conclusions obtained from previous sensitivity studies in similar nozzles performed by the authors [2,4,15–17, 22]. These studies established that the cell size in the orifice must grow from 1.15 µm in the vicinity of the wall up to 7 µm in the centre of the orifice. For the rest of the domain (upstream of the orifice) a cell size of 22.5 µm is enough to ensure the coherence and accuracy of all the flow variables calculated (velocity, pressure, density, turbulent kinetic energy, energy dissipation, etc.). The meshes have been constructed following these recommendations. As example, the mesh for the nozzle CD-2.5 is showed in Figure 2. The resulting meshes have around 240 000 hexahedral cells.

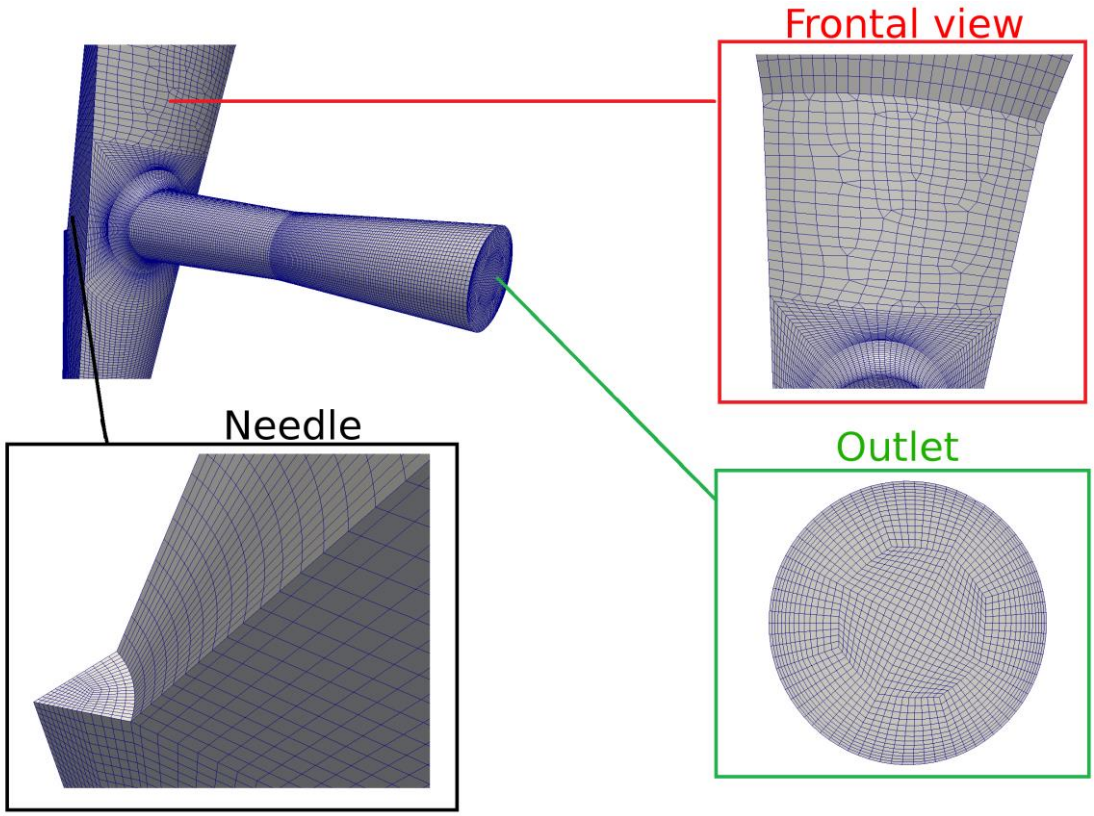

Figure 2: Example of the mesh structure for CD-2.5.

For the simulations, as displayed in Fig. 1, a fixed pressure condition has been used at the inlet where the injection pressure (P_{in}) is set, whereas a mean pressure conditions has been established for the outlet, where the back-pressure is set (P_b). This mean pressure condition in the orifice outlet keeps the mean desirable value, allowing zones with very low pressure because of the presence of vapour in the flow. At the walls, a non-slip condition has been used for the velocity. The study has been performed at an injection pressure of 40 MPa and over a backpressure swept from 1 MPa to 25 MPa, as displayed in Table 2.

Injection pressure [MPa]	Backpressure [MPa]
40	1, 3, 5, 7, 9, 11, 13, 15, 17, 19, 21, 23, 25

Table 2: Test matrix.

4. RESULTS AND ANALYSIS.

4.1 Flow parameters

The nozzles have been compared by using the following flow parameters: mass flow Eq. (22), momentum flux Eq. (23) and effective velocity Eq. (24). All of them have been evaluated at the nozzle exit:

$$\dot{m}_{\mathrm{f}} = \int \rho \, (\vec{u} \cdot \vec{n}) \, dS \tag{22}$$

$$\dot{M}_{\mathrm{f}} = \int \rho (\vec{u} \cdot \vec{n})^2 dS \tag{23}$$

$$u_{\mathrm{eff}} = \frac{\dot{M}_{\mathrm{f}}}{\dot{m}_{\mathrm{f}}} \tag{24}$$

where ρ is the density, $\vec{u}$ the velocity and $\vec{n}$ the normal vector to the surface S (in this case the outlet section).

4.2 Mass flow analysis and cavitation inception detection.

Fig. 3, in the upper part (left), shows the mass flow against the square root of the pressure differential for the three tested nozzles. Each point corresponds to a different backpressure. As can be seen, the nozzle CD-4.5, with highest convergence-divergence level according to Table 1, presents the highest mass flow for all the injection conditions, whereas, the nozzle with lowest convergence-divergence level has the lowest mass flow. Aside from the differences found between nozzles in terms of mass flow, a different behaviour can be observed when comparing the nozzles. Taking the nozzle CD-2.5 as a reference, the mass flow increases linearly with the square root of the pressure differential until a point where it stabilizes. At this point, a flow chocking occurs, which means that it remains unchanged whichever the backpressure. Pressure conditions needed to reach this situation are called critical cavitation conditions (*CCC*). The detection of the

beginning of mass flow chocking is often used to experimentally detect cavitation in real nozzles [5]. The critical cavitation conditions are represented in Fig. 3 as *CCC* for the three nozzles. The *CCC* is related to the critical backpressure needed to induce the nozzle to cavitate. The higher the backpressure needed for cavitation inception (critical backpressure), the more likely the nozzle is to cavitate. In fact, it cavitates for backpressures equal or lower than the critical backpressure. Obviously, from that value, the lower the backpressure, the higher the cavitation intensity.

According to this, the nozzle with highest level of convergence-divergence (CD-4.5) is the most prone to cavitate, followed by the one with an intermediate level of convergence-divergence (CD-3.5) and finally, the one with the lowest level of convergence-divergence. In fact, the nozzle CD-4.5 is cavitating for all backpressures tested, i.e., the mass flow is always chocked, whichever the backpressure.

4.3 Comparison in terms of momentum flux and effective velocity.

In the upper part of Fig. 3 (right) the momentum flux for the analysed injection pressure and all the tested backpressures is depicted against the square root of pressure drop for all the nozzles. As can be seen, in all the cases, the momentum flux increases with the square root of pressure drop. Nevertheless, unlike previous mass flow results, momentum flux does not suffer any collapse with cavitation inception and development [2, 4, 8]. With the values of mass flow and momentum flux, the effective velocity can be obtained dividing the momentum flux by the mass flow according to Eq. (24). The effective velocity obtained by this way is displayed in the bottom part of Fig. 3. Taking as a sample the nozzle with lowest convergence-divergence level (CD-2.5), it is easy to appreciate an increase in the slope in the velocity points when cavitating conditions are reached. For

this nozzle, the *CCC* point is located around 4600 $Pa^{0.5}$. It means that the backpressure for reaching cavitation inception is around 19 MPa. Thus the value of $\sqrt{\Delta P} = \sqrt{(P_{\mathrm{in}} - P_{\mathrm{b}})} = \sqrt{(400 - 190) \cdot 10^5} \approx 4600\ \mathrm{Pa}^{0,5}$. For higher values of $\sqrt{\Delta P}$, the nozzle cavitates and the change in the slope means that the increment in effective velocity is higher than expected if only the increment of pressure drop was considered. This fact is shown in the velocity graph by the deviation between continuous line and points for $\sqrt{\Delta P} > 4600$. This result is well known in literature and it is one of the most important consequences of cavitation ([2], [4], [8], [10], [15], [24]). It is due to the viscosity reduction in the zone occupied by the vapour phase along the orifice wall, which reduces the friction zone in the channel [2]. If a comparison of the nozzles is made in terms of effective velocity, it can be observed that, in general terms, for the conditions tested, the highest effective velocities are achieved for the nozzle with the lowest level of convergence-divergence. Nevertheless, the differences between nozzles are reduced at high pressure drops (i.e. low backpressures) for which cavitation intensity is higher in the nozzles with higher level of convergence-divergence. The higher increase in the injection velocity due to the higher cavitation intensity in these nozzles compensates to a certain degree the small velocities expected due to the higher geometrical area at the nozzle outlet.

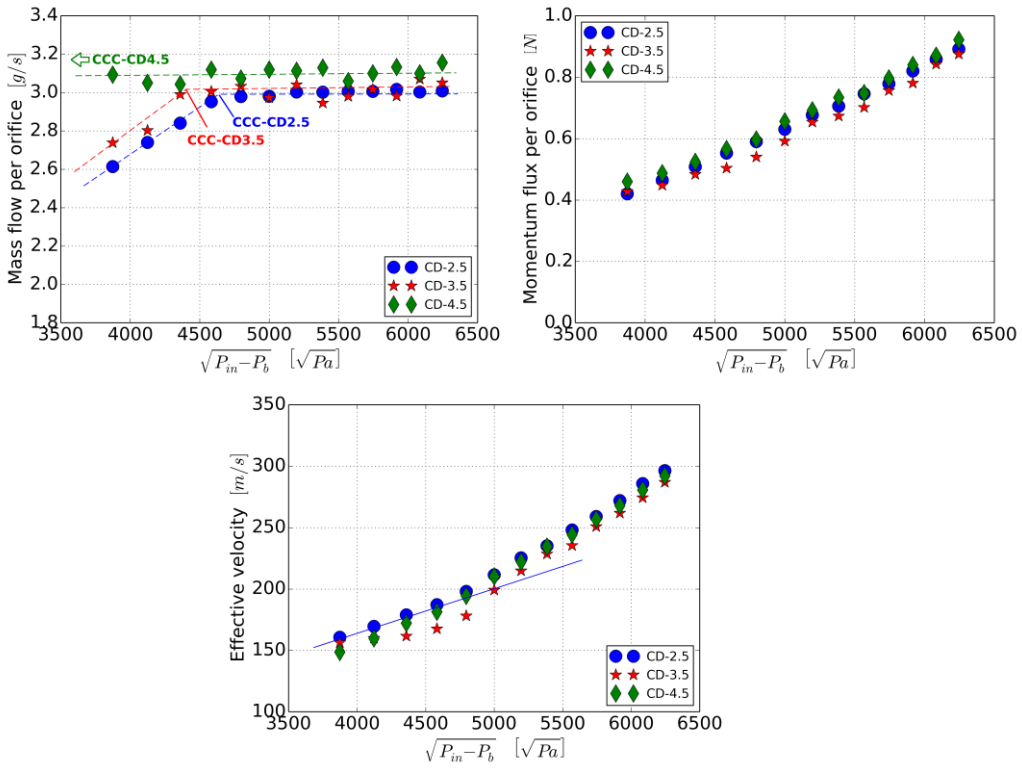

Figure 3. Flow parameters

4.4 Cavitation morphology

To compare the morphology of the cavitation pattern in the three nozzles, mean images of the vapour distribution along the orifices of the different nozzles are displayed in Fig. 4. In the Figure, the zones with vapour mas fraction (γ) between 0 and 1 are represented. The results belong to three different backpressures (1 MPa, 13 MPa and 25 MPa). As it can be observed in this Figure, cavitation zones are mainly located in the divergent part, after the throttle in the midpoint of the orifice. In the first convergent part, cavitation is mainly avoided, except for the nozzle with lowest level of conicity. It is well known that convergent (conical) orifices prevent nozzles from cavitating due to the smoother pressure change along the orifice induced by this geometry compared to cylindrical ones [1].

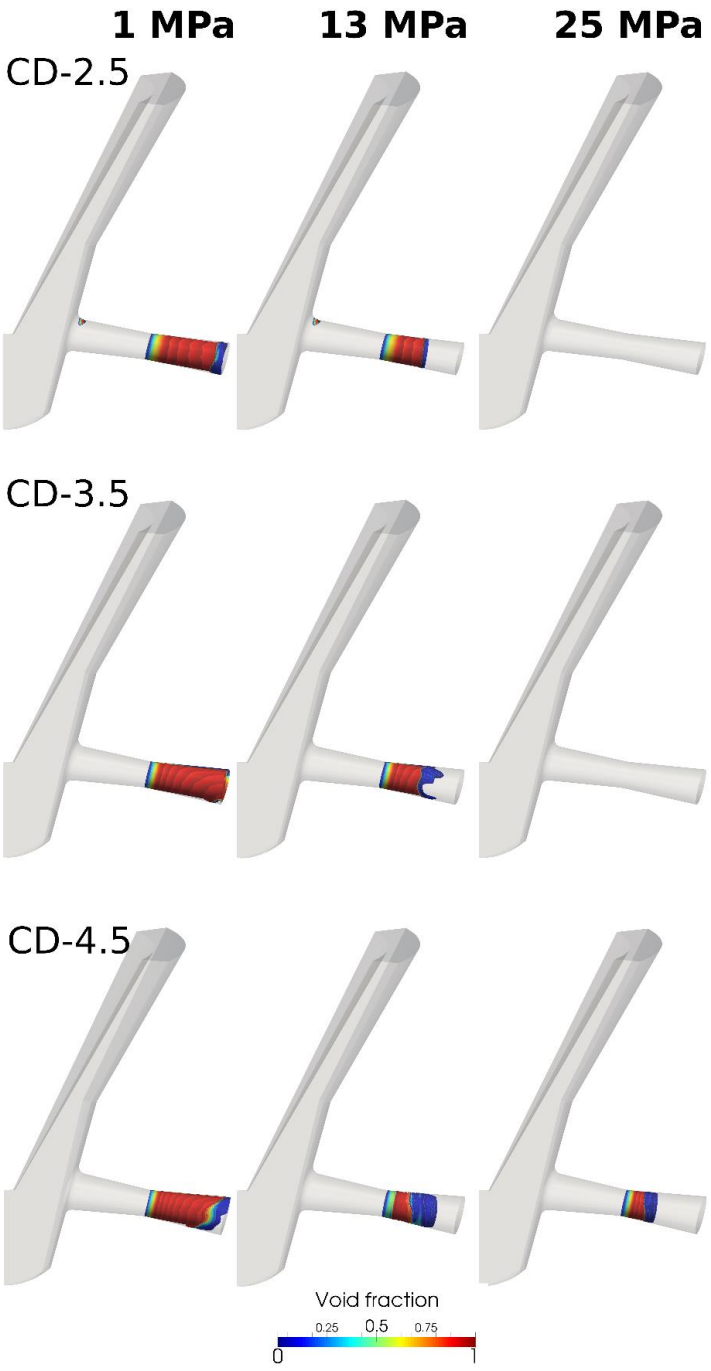

Figure 4. Cavitation morphology.

This remark is consistent with the cavitation pattern in the first convergent part of the nozzle for the nozzle CD-2.5. In this nozzle, with lowest conicity level, cavitation phenomenon occurs as well in the rounding radius at the orifice inlet, but it does not

spread along the wall. In the other cases (CD-3.5 and CD-4.5) cavitation is totally avoided in this first convergent part of the nozzle due to the higher degree of conicity.

However, opposite of what happen in the first convergent part, the higher the divergence level in the second part of the orifice, the higher the intensity of cavitation. This result can be clearly seen in Fig. 4, especially for the backpressure of 25 MPa, at which cavitation is avoided in the nozzles CD-2.5 and CD-3.5, but it remains in nozzle CD-4.5.

4.5 Comparison in terms of flow coefficients.

Flow coefficients are useful to analyse the flow behaviour. The first one, the discharge coefficient, is representative of the global losses in the nozzle. It is obtained dividing the mass flow by a theoretical mass flow (Eq. (25)). The theoretical mass flow in the denominator takes into account the theoretical velocity according to Bernoulli's equation Eq. (26):

$$C_{\mathrm{d}} = \frac{\dot{m}_{\mathrm{f}}}{\rho A_{\mathrm{O}} u_{\mathrm{th}}} \tag{25}$$

$$u_{\mathrm{th}} = \sqrt{\frac{2(P_{\mathrm{in}} - P_{\mathrm{b}})}{\rho}} \tag{26}$$

The second non-dimensional flow parameter is the velocity coefficient, C_{v}, which relates the effective velocity to the maximum theoretical Bernoulli´s velocity, u_{th}:

$$C_{\mathrm{v}} = \frac{u_{\mathrm{eff}}}{u_{\mathrm{th}}} \tag{27}$$

where the effective velocity can be calculated by dividing the momentum flux by the mass flow as was established by Eq. (24).

The third flow coefficient, the contraction coefficient, C_a, is used to evaluate the reduction of the effective area with regard to the geometric one due to the presence of vapour bubbles (originated by cavitation) into the flow that reach the orifice outlet:

$$C_{\mathrm{a}} = \frac{A_{\mathrm{eff}}}{A_0} = \frac{\dot{m}^2}{\rho \dot{M} A_0} \tag{28}$$

These flow parameters are related to each other by means of Eq. (29):

$$C_{\mathrm{d}} = C_{\mathrm{v}} C_{\mathrm{a}} \tag{29}$$

Fig. 5 displays the discharge coefficient, velocity coefficient and area coefficient for all nozzles against the square root of the pressure drop.

With regard to the discharge coefficient, in the cavitating zone, due to the mass flow collapse, the discharge coefficient experiences an abrupt drop. This drop starts at the point corresponding to the cavitation inception (recall *CCC* in Fig. 3). A lower critical cavitation conditions (in terms of square root of pressure drop) means that, for the considered injection pressure, the backpressure needed to produce cavitation inception is higher. A lower critical pressure drop implies that the discharge coefficient fall due to cavitation begins at lower pressure drops. Thus, if the discharge coefficients are compared for a given pressure drop in cavitating conditions, the lowest values are obtained for nozzle CD-4.5, and the highest for CD-2.5 which is compatible with higher cavitation intensity showed by the nozzle CD-4.5, followed by CD-3.5 and finally CD-2.5. This behaviour will have an impact on the area and effective velocity coefficients, as it will be seen next.

As seen in the bottom part of Fig. 5, the area coefficient takes values equal to one in non-cavitating conditions. Therefore, for these conditions, the velocity coefficient values, displayed in the upper part of Fig. 5 (right), equal the discharge coefficient ones. As was the case for the discharge coefficient, the area coefficient falls once the cavitation starts. The fact that the nozzle differ on the critical pressure conditions from which this phenomenon starts to occur, makes that as it happened to the discharge coefficient, for a given pressure drop higher than the critical one, CD-4.5 followed by CD-3.5 nozzles exhibit the lower values of this coefficient. The velocity coefficient behaviour is in agreement with the results just analysed (recall Eq. (29)). Its value equals the discharge coefficient for non-cavitating conditions, since the area coefficient equals the unity. In cavitating conditions, its increase is greater the higher the cavitation intensity is. Therefore, as commented for the effective velocity, as the cavitation phenomenon develops, the values of the velocity coefficient for the nozzle with the highest convergence-divergence level (CD-4.5) reach almost the ones observed for the lowest level (CD-2.5).

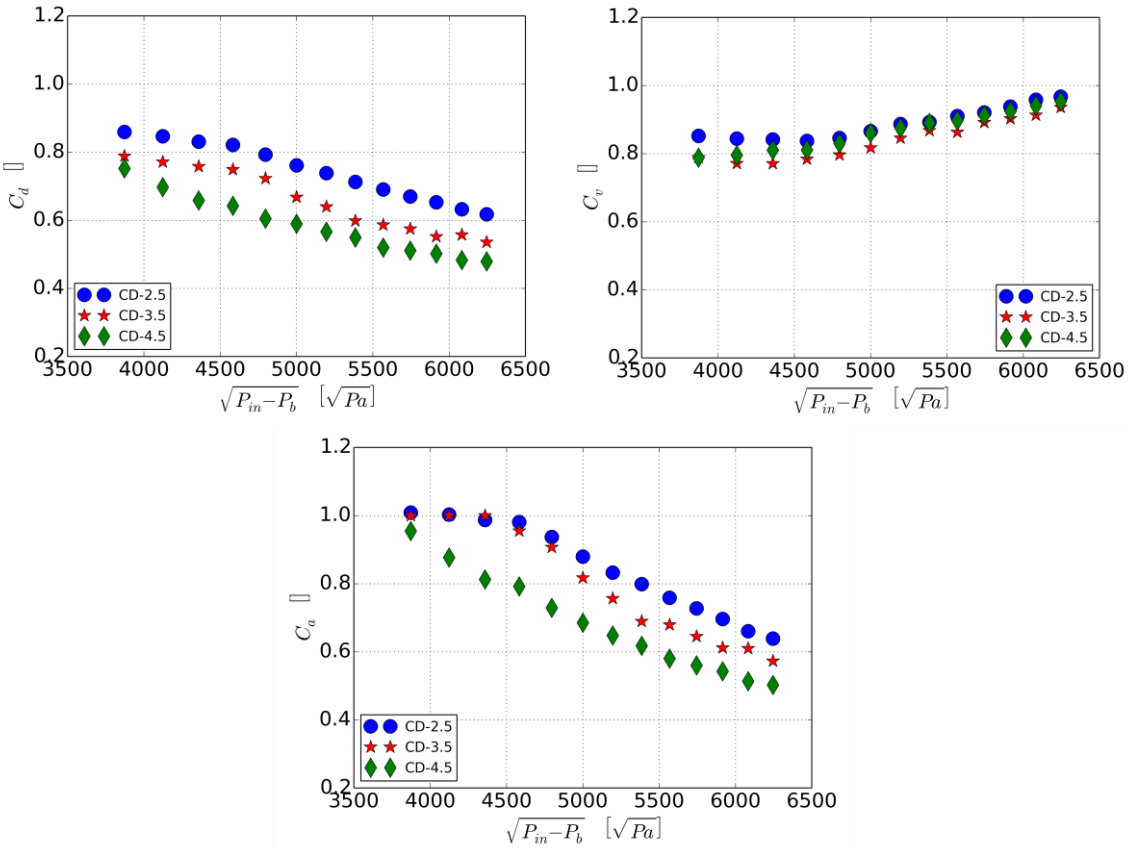

Figure 5: Dimensionless flow coefficients.

4.6 Air-fuel mixing process estimation.

In previous results, it has been seen that the cavitation provokes a substantial increase on the effective velocity. As a result, the effective injection velocity for the nozzles with higher convergence-divergence level, despite of their higher outlet geometrical area, could take similar values than those observed for the nozzle with lower convergence-divergence level. On the other hand, it is well known from previous studies in the literature that cavitation produces an important increase of the spray spreading angle [23–25]. Additionally, aside from the influence of cavitation on the spray cone angle, the nozzles with higher convergence-divergence level are supposed to have higher spray cone angle due to the divergence in the final part of the orifice. Attending to the "similar"

injection effective velocity observed for the nozzles, the cavitation susceptibility and its consequences on the spray spreading angle and this last remark, a qualitative order on the mixing process quality could be established. This can be done since the air-fuel mixing process depends on the injection velocity and the spray cone angle [5]. Taking into account all the results, in general terms, everything seems to point to a better mixing process for the nozzle with highest convergence-divergence level and a worse process for the nozzle with lowest convergence-divergence level. Nevertheless further experimental characterization of these nozzles is needed in order to confirm the results obtained from this computational research. Furthermore, from the point of view of numerical simulations, further investigations aiming at evaluating these kind of nozzles in more realistic transient conditions are also needed to verify whether the conclusions obtained here could be extrapolated to such conditions. For that, simulations at partial needle lifts [4] or moving mesh algorithm simulating needle lift profiles are essential.

5. CONCLUSIONS

The main conclusions of this study are drawn in the following points:

- The higher the convergence-divergence level of the nozzle, the higher the mass flow and the momentum flux.
- The nozzles with higher convergence-divergence level are more prone to cavitate and in these nozzles the cavitation vapour is generated in the throttle of the orifice (at midpoint), spreading along the wall of the divergence part.
- Despite of their higher outlet geometrical area, the nozzles with higher convergence-divergence level present slightly smaller effective injection velocity

than the nozzles with lower convergence-divergence level for the injection conditions analysed (injection pressure of 40 MPa and different backpressures)

- Attending to the injection effective velocity values for the different nozzles and the cavitation susceptibility and its consequences on the spray spreading angle, a better mixing process is expected for the nozzle with highest convergence-divergence level and a worse mixing process is expected for the nozzle with lowest convergence-divergence level.

ACKNOWLEDGMENTS

This work was partly sponsored by "Ministerio de Economía y Competitividad" of the Spanish Government, in the frame of the project "Estudio de la interacción chorro-pared em condiciones realistas de motor", Reference TRA2015-67679-c2-1-R. This support is gratefully acknowledged by the authors.

Mr. Jaramillo´s thesis is supported by "*Conselleria d'Educació, Cultura I Esports" of "Generalitat Valenciana*" through the program "*Programa VALI+D para investigadores en Formación*", Reference ACIF/2015/040.

The authors would like to express gratitude for the computer resources, technical expertise and assistance provided by the Universidad de Valencia relating to the use of the supercomputer "Tirant".

NOMENCLATURE

A_{eff} outlet effective area

A_o outlet area

C_a area coefficient

C_d discharge coefficient

C_v velocity coefficient

$C_{\varepsilon 1}$ constant for ε transport equation calculation

$C_{\varepsilon 2}^{o}$ variable for ε transport equation calculation

$C_{\varepsilon 2}$ constant for ε transport equation calculation

C_μ constant for turbulent viscosity calculation

c speed of sound

D_i diameter at the orifice inlet

D_{mid} diameter at the middle of the orifice

D_o diameter at the orifice outlet

K cavitation number

k turbulent kinetic energy

k-factor conicity factor

L orifice length

$\dot{M}_f$ momentum flux

$\dot{m}_f$ mass flow

P pressure

P_b discharge back pressure

P_{in} injection pressure

P_{vap} vaporisation pressure

p_k production of turbulent kinetic energy

r rounding radius at the inlet orifice

t time

$\vec{u}$ velocity

$\bar{u}$ averaged velocity

u' fluctuating velocity

u_{eff} effective velocity

u_{th} theoretical velocity

S mean strain

S_{ij} strain tensor

GREEK SYMBOLS:

ΔP pressure drop, $\Delta P = P_{in} - P_b$

Ψ fluid compressibility

Ψ_l liquid compressibility

Ψ_v vapour compressibility

α_ε constant for ε transport equation calculation

α_k constant for *k* transport equation calculation

β constant for the turbulence model

γ vapour mass fraction

ε turbulence dissipation rate

μ fluid viscosity

μ_l liquid viscosity

μ_T turbulent viscosity

μ_v vapour viscosity

η expansion parameter

η_0 constant for the turbulence model

ρ fluid density

ρ_l liquid density

$\rho_{l,sat}$ liquid density at saturation

ρ_l^o liquid density at a given temperature condition

$\rho_{v,sat}$ vapour density at saturation

ρ_v vapour density

θ nozzle angle

REFERENCES

[1] J. M., Desantes, F. J. Salvador, J. J. López, J. De la Morena, Study of mass and momentum transfer in diesel sprays based on X-ray mass distribution measurements and on a theoretical derivation. Experiments in Fluids, 50(2), (2011), 233–246. http://doi.org/10.1007/s00348-010-0919-8

[2] F. Payri, R. Payri, F.J. Salvador, J. Martínez-López, A contribution to the understanding of cavitation effects in Diesel injector nozzles through a combined experimental and computational investigation, Comput. Fluids. 58 (2012) 88–101. doi:10.1016/j.compfluid.2012.01.005.

[3] J.M. Luján, B. Tormos, F.J. Salvador, K. Gargar, Comparative analysis of a DI diesel engine fuelled with biodiesel blends during the European MVEG-A cycle: Preliminary study (I), Biomass and Bioenergy. 33 (2009) 941–947. doi:10.1016/j.biombioe.2009.02.004.

[4] F.J. Salvador, J. Martínez-López, M. Caballer, C. De Alfonso, Study of the influence of the needle lift on the internal flow and cavitation phenomenon in diesel injector nozzles by CFD using RANS methods, Energy Convers. Manag. 66 (2013) 246–256. doi:10.1016/j.enconman.2012.10.011.

[5] R. Payri, F.J. Salvador, J. Gimeno, J. De la Morena, Influence of injector technology on injection and combustion development – Part 2: Combustion

analysis, Appl. Energy. 88 (2011) 1130–1139. doi:10.1016/j.apenergy.2010.10.004.

[6] C.M. Ho, E. Gutmark, Vortex induction and mass entrainment in a small-aspect-ratio elliptic jet, J. Fluid Mech. 179 (1987) 383–405.

[7] F. Hussain, H.S. Husain, Elliptic jets. Part 1. Characteristics of unexcited and excited jets, J. Fluid Mech. 208 (1989) 257–320.

[8] S. Molina, F.J. Salvador, M. Carreres, D. Jaramillo, A computational investigation on the influence of the use of elliptical orifices on the inner nozzle flow and cavitation development in diesel injector nozzles, Energy Convers. Manag. 79 (2014) 114–127. doi:10.1016/j.enconman.2013.12.015.

[9] G. Yunyi, L. Changwen, H. Yezhou, P. Zhijun, An Experimental Study on Droplet Size Characteristics and Air Entrainment of Elliptic Sprays, SAE Paper 982546 (1998). doi:10.4271/982546.

[10] J.G. Hong, K.W. Ku, S.R. Kim, C.W. Lee, Effect of cavitation in circular nozzle and elliptical nozzles on the spray characteristic, At. Sprays. 20 (2010) 877–886.

[11] A. Matsson, L. Jacobsson, S. Andersson, The Effect of Elliptical Nozzle Holes on Combustion and Emission Formation in a Heavy Duty Diesel Engine, SAE Paper 200-01-125 (2000). doi:10.4271/2000-01-1251.

[12] C.-C. Hu, W.-T. Lin, C.-M. Su, W.-J. Liu, Discharge characteristics of small sonic nozzles in the shape of pyramidal convergent and conical divergent, Flow Meas. Instrum. 25 (2012) 26–31. doi:10.1016/j.flowmeasinst.2011.08.006.

[13] J. Liu, J. Chen, Z. Chen, Critical flashing flow in convergent–divergent nozzles with initially subcooled liquid, Int. J. Therm. Sci. 47 (2008) 1069–1076. doi:10.1016/j.ijthermalsci.2007.07.019.

[14] OPENFOAM® is a registered trade mark of OpenCFD Limited, (2015). http://www.openfoam.com.

[15] F.J. Salvador, J.-V. Romero, M.-D. Roselló, J. Martínez-López, Validation of a code for modeling cavitation phenomena in Diesel injector nozzles, Math. Comput. Model. 52 (2010) 1123–1132. doi:10.1016/j.mcm.2010.02.027.

[16] F.J. Salvador, S. Hoyas, R. Novella, J. Martinez-Lopez, Numerical simulation and extended validation of two-phase compressible flow in diesel injector nozzles, Proc. Inst. Mech. Eng. Part D J. Automob. Eng. 225 (2011) 545–563. doi:10.1177/09544070JAUTO1569.

[17] F.J. Salvador, J. Martínez-López, J.-V. Romero, M.-D. Roselló, Computational study of the cavitation phenomenon and its interaction with the turbulence developed in diesel injector nozzles by Large Eddy Simulation (LES), Math. Comput. Model. 57 (2013) 1656–1662. doi:10.1016/j.mcm.2011.10.050.

[18] T.J. Chung, Computational Fluid Dynamics, Cambridge University Press, Cambridge, 2010. doi:10.1017/CBO9780511780066.

[19] H. Bruce Stewart, B. Wendroff, Two-phase flow: Models and methods, J. Comput. Phys. 56 (1984) 363–409. doi:10.1016/0021-9991(84)90103-7.

[20] V. Yakhot, S.A. Orszag, S. Thangam, T.B. Gatski, C.G. Speziale, Development

of turbulence models for shear flows by a double expansion technique, Phys. Fluids A. 4 (1992) 1510–1520.

[21] C., Bae, J., Yu, J. Kang, J., Kong, Effect of Nozzle Geometry on the Common-Rail Diesel Spray. SAE Technical Paper 2002-01-1625. (2002).

[22] F.J. Salvador, J. Martínez-López, J.-V. Romero, M.-D. Roselló, Influence of biofuels on the internal flow in diesel injector nozzles, Math. Comput. Model. 54 (2011) 1699–1705. doi:10.1016/j.mcm.2010.12.010.

[23] F. Payri, V. Bermúdez, R. Payri, F.J. Salvador, The influence of cavitation on the internal flow and the spray characteristics in diesel injection nozzles, Fuel. 83 (2004) 419–431. doi:10.1016/j.fuel.2003.09.010.

[24] A. Sou, S. Hosokawa, A. Tomiyama, Effects of cavitation in a nozzle on liquid jet atomization, Int. J. Heat Mass Transf. 50 (2007) 3575–3582. doi:10.1016/j.ijheatmasstransfer.2006.12.033.

[25] S. Som, S.K. Aggarwal, E.M. El-Hannouny, D.E. Longman, Investigation of Nozzle Flow and Cavitation Characteristics in a Diesel Injector, J. Eng. Gas Turbines Power. 132 (2010) 042802. doi:10.1115/1.3203146.

[26] F. J. Salvador, M. Carreres, D. Jaramillo, J. Martínez-López, J. Analysis of the combined effect of hydrogrinding process and inclination angle on hydraulic performance of diesel injection nozzles. Energy Conversion and Management, 105 (2015), 1352–1365. doi:10.1016/j.enconman.2015.08.035

[27] F. J. Salvador, M. Carreres, D. Jaramillo, J. Martínez-López, J. Comparison of

microsac and VCO diesel injector nozzles in terms of internal nozzle flow characteristics. Energy Conversion and Management, 103 (2015), 284–299. doi:10.1016/j.enconman.2015.05.062

[28] J. M., Desantes, F. J. Salvador, M. Carreres, J. Martinez-Lopez, J. Large-eddy simulation analysis of the influence of the needle lift on the cavitation in diesel injector nozzles. Proceedings of the Institution of Mechanical Engineers, Part D: Journal of Automobile Engineering, 229(4) (2014), 407–423. doi:10.1177/0954407014542627

[29] J. J. López, F. J. Salvador, O. de la Garza, J. Arrègle. A comprehensive study on the effect of cavitation on injection velocity in diesel nozzles. Energy Conversion and Management, 64 (2012), 415–423. doi:10.1016/j.enconman.2012.03.032

[30] F. J. Salvador, J.-V. Romero, M.-D. Roselló, D. Jaramillo. Numerical simulation of primary atomization in diesel spray at low injection pressure. Journal of Computational and Applied Mathematics, 291 (2015), 94–102. doi:10.1016/j.cam.2015.03.044